

Enhancement of Structural and Optical Properties of Porous $\text{In}_{0.27}\text{Ga}_{0.73}\text{N}$ Thin Film Synthesized Using Electrochemical Etching Technique

Saleh H. Abud^{1,2,*}, Z. Hassan¹, F. K. Yam¹

¹ Nano-Optoelectronics Research and Technology (N.O.R) Laboratory, School of Physics, Universiti Sains Malaysia, 11800 Penang, Malaysia.

² Department of Physics, College of Science, University of Kufa, Kufa, Najaf, Iraq.

* E-mail: Salehhasan71@gmail.com

Received: 11 August 2012 / Accepted: 19 September 2012 / Published: 1 October 2012

This paper presents the growth conditions of $\text{In}_{0.27}\text{Ga}_{0.73}\text{N}/\text{Si}(111)$ thin film with thickness of 110 nm prepared using plasma-assisted molecular beam epitaxy technique. Indium mole fraction of 0.27 was calculated using X-ray diffraction and Vegard's law. Some ridges on the film were observed on the as-grown surface morphology. Furthermore, porous $\text{In}_{0.27}\text{Ga}_{0.73}\text{N}$ structure was synthesized using UV-assisted electrochemical etching technique with various current densities. Formed pores were dissimilar in terms of shape and size because of changes in the etching current density. Crystallite size and the strain inside the film were calculated for both as-grown and porous $\text{In}_{0.27}\text{Ga}_{0.73}\text{N}$. The result shows that both crystallite size and compressive strain decreased with increasing current density. A slight blue shift of porous $\text{In}_{0.27}\text{Ga}_{0.73}\text{N}$ regarding the wavelength of the as-grown film was observed at 554 and 553.1 nm by using photoluminescence measurements. Finally, a Raman phonon mode of $A_1(\text{LO})$ at 625.6 cm^{-1} of the as-grown film was observed. However, a shift towards higher frequency was monitored in the porous $\text{In}_{0.27}\text{Ga}_{0.73}\text{N}$ film.

Keywords: Porous InGaN; PA-MBE; HR-XRD; Photoluminescence.

1. INTRODUCTION

The InGaN ternary alloy system receives a great deal of attention among III-nitride compound semiconductors because of its direct band gap tuning from 0.7 eV for InN to 3.4 eV for GaN, giving InGaN great potential for the design of high-efficiency optoelectronic devices that operate in the IR, visible, and UV regions of the electromagnetic spectrum [1].

Porous III-nitride compounds are considered as promising materials for optoelectronics [2] and chemical and biochemical sensors [3] because of their unique optical and electronic properties compared with bulk materials [4, 5]. The formation of a porous nanostructure has been widely reported for crystalline silicon [6]. In addition to porous silicon research, attention has also been focused on other porous semiconductors, such as GaAs [7] and GaN [8-10]. Interest in porous semiconductor materials arises from the fact that these materials can act as sinks for threading dislocation and are able to accommodate strain. Porous semiconductor materials are also useful for understanding the fundamental properties of nanoscale structures for the development of nanotechnology. Research on porous GaN is strongly driven by the robustness of porous GaN, including its excellent thermal, mechanical, and chemical stabilities that make it highly desirable for optical applications [11]. Many researchers [4, 12-14] have used the photoelectrochemical etching (PEC) technique to synthesize porous GaN. The PEC technique is more suitable and cheaper compared with other techniques for producing high-density nanostructures with controlled pore size and shape [4]. Electrolyte, current density and illumination are the main factors that affect electrochemical etching. Hydrofluoric acid (HF) is the most commonly used material in etching GaAs and GaN [15]. In the current study, the PEC technique is used to synthesize porous InGaN nanostructures at various current densities.

To the best of our knowledge, this study is the first to report on the synthesis of porous InGaN by using the PEC technique.

2. EXPERIMENTAL PROCEDURE

2.1. Growth of $In_{0.27}Ga_{0.73}N$ thin film

$In_{0.27}Ga_{0.73}N/GaN/AlN$ epitaxial layers were grown on Si(111) substrate by using a plasma-assisted molecular beam epitaxy (PA-MBE) system (Veeco Gen II). High-purity sources, such as gallium (7N), aluminum (6N5), and indium (7N), were installed in the Knudsen cells. Reactive nitrogen species were generated by channeling high-purity nitrogen to a radio frequency (RF) source. The resultant nitrogen plasma was at a nitrogen pressure of 1.5×10^{-5} Torr under 300 W rated discharge power. The Si(111) wafer (3 inches) was cleaned using the Radio Corporation of America (RCA) method prior to the loading of the substrate to the PA-MBE system. The substrate was outgassed in the load-lock and buffer chamber after being loaded into the PA-MBE system, and then it was transferred to the growth chamber. Surface treatment was conducted on the substrate to ensure the absence of SiO_2 , leaving only clean Si substrate. This process was done by depositing a few monolayers of Ga on the substrate at 750 °C, resulting in the formation of Ga_2O_3 . The clean Si surface was further confirmed by the presence of prominent Kikuchi lines that were observed using reflection high-energy diffraction. A few monolayers of Al were deposited on the Si surface prior to the growth of nitride layers to inhibit the formation of Si_xN_y , which is detrimental to the growth of subsequent epitaxy layers. An AlN buffer layer was deposited by setting Al and N shutters to open simultaneously for 15 min. The GaN layer was then deposited on the buffer layer at a substrate temperature of 800 °C for 33 min. Finally, the substrate temperature was reduced to 700 °C, and the In and Ga effusion cells

were heated to 925 and 930 °C, respectively, to initiate the growth of InGaN. The final growth process lasted for approximately 30 min.

2.2. Synthesis of porous InGaN nanostructure

Porous In_{0.27}Ga_{0.73}N was produced using the UV-PEC method. The etching cell was made from Teflon with platinum wire as cathode and In_{0.27}Ga_{0.73}N film as anode. The native oxide of the samples was initially removed using NH₄OH:H₂O (1:20), followed by HF:H₂O (1:50). Boiling aqua regia HCl:HNO₃ (3:1) was subsequently used to clean the samples. The samples were then etched in a solution of HF(49%):C₂H₅OH(99.99%) with a ratio of 1:5 under UV lamp illumination at two different current densities of 25 and 50 mA/cm² for 15 min. All samples were rinsed with ethanol after the etching process, and were then dried using nitrogen gas. All experimental processes were conducted at room temperature.

2.3. Characterization

The surface morphology of the as-grown and porous In_{0.27}Ga_{0.73}N thin films were performed using field emission scanning electron microscopy (FESEM, Model FEI Nova NanoSEM 450) and noncontact atomic force microscopy (AFM, Model Dimension EDGE, BRUKER). Structural properties were investigated using high-resolution X-ray diffraction (HR-XRD, Model PANalytical X'Pert POR MRD PW3040) with Cu K_α radiation wavelength of 0.154 nm. Finally, optical properties were assessed using photoluminescence (PL) and Raman spectroscopy (Model Jobin Yvon HR 800 UV) excited by He-Cd laser at 325 nm and argon ion laser at 514.5 nm, respectively.

3. RESULTS AND DISCUSSION

Figs. 1(A)–1(D) show the FESEM images of the as-grown and etched In_{0.27}Ga_{0.73}N films. Fig. 1(A) shows some of the formed ridges on the as-grown surface, which can be attributed to the lattice mismatch and thermal mismatch between the buffer AlN layer and the Si substrates. Fig. 1(B) shows the cross-section image of the as-grown sample, in which the thicknesses of the layers were estimated to be 110, 125, and 85 nm for In_{0.27}Ga_{0.73}N, GaN, and AlN, respectively. Fig. 1(C) shows the etching current density effect of 25 mA/cm² at 15 min on the surface morphology of In_{0.27}Ga_{0.73}N film. Irregular pores with different shapes and sizes were observed. Fig. 1(D) shows the effect of increasing the current density to 50 mA/cm² on the surface morphology in terms of the shape and size of the formed pores. The pores were more regular in shape and their number decreased with increasing current density, whereas average pore size increased twice with respect to Fig. 1(C). This finding indicates that pore size increases and grain size decreases when the current density is increased from 25 mA/cm² to 50 mA/cm².

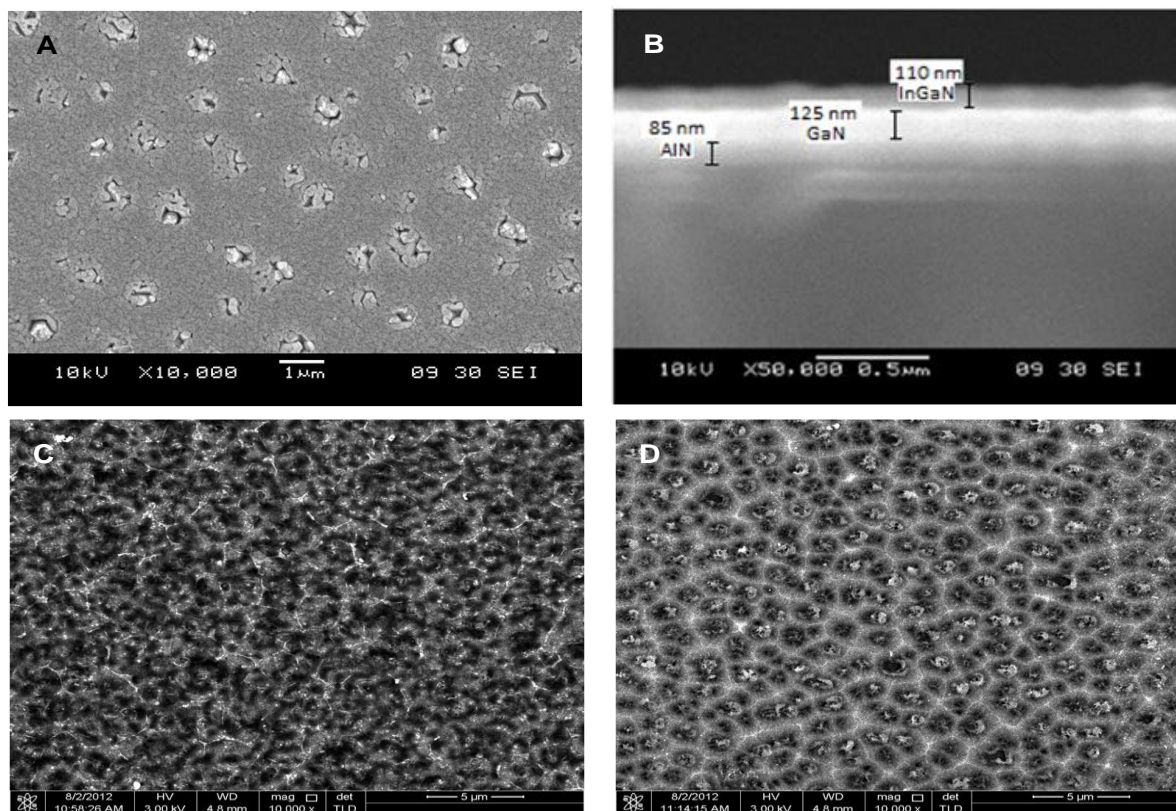


Figure 1. FESEM image of the as-grown and porous InGaN formed at different current densities. (A) as-grown, (B) cross section of the as-grown, (C) 25mA/cm², (D) 50mA/cm².

Figs. 2(A)–2(C) show 3D-AFM images of the as-grown and etched films. Fig. 2(A) shows the as-grown surface, in which ridges formed on the surface. This observation is in agreement with the FESEM results in Fig. 1(A). Figs. 2(B) and 2(C) show the effect of rising current density on the surface morphology of the etched films. As can be seen in Fig. 2(B), the current density of 25 mA/cm² had insignificant effect on the surface morphology of the etched film. However, the root mean square (RMS) increases from 12.2 nm for the as-grown film to 15.3 nm for the etched film. Fig. 2(C) shows the considerable influence of the increment of 50 mA/cm² in current density on the surface morphology of the etched film when the RMS increased to 19.2 nm. This finding indicates that the roughness of the surface increases with increasing current density.

Figs. 3(A) and 3(B) show the X-ray diffraction (XRD) patterns of the as-grown and porous In_{0.27}Ga_{0.73}N thin films at various current densities. In Fig. 3(A), the diffraction peaks were located at 33.61°, 34.54°, and 36.02° relative to the (0002) In_{0.27}Ga_{0.73}N, GaN, and AlN films, respectively. No diffraction peak of InN was observed, indicating that no phase segregation occurred. The intensity of the In_{0.27}Ga_{0.73}N diffraction peak was significantly lower than that of GaN, indicating that the In_{0.27}Ga_{0.73}N film is thinner than the GaN film [12] and that a large full width at half maximum (FWHM) weakens the peak intensity. Fig. 3(B) shows a broadening diffraction peak of the porous In_{0.27}Ga_{0.73}N films, which implies a reduction in crystallite size, as confirmed by the Scherrer equation (Eq. 3).

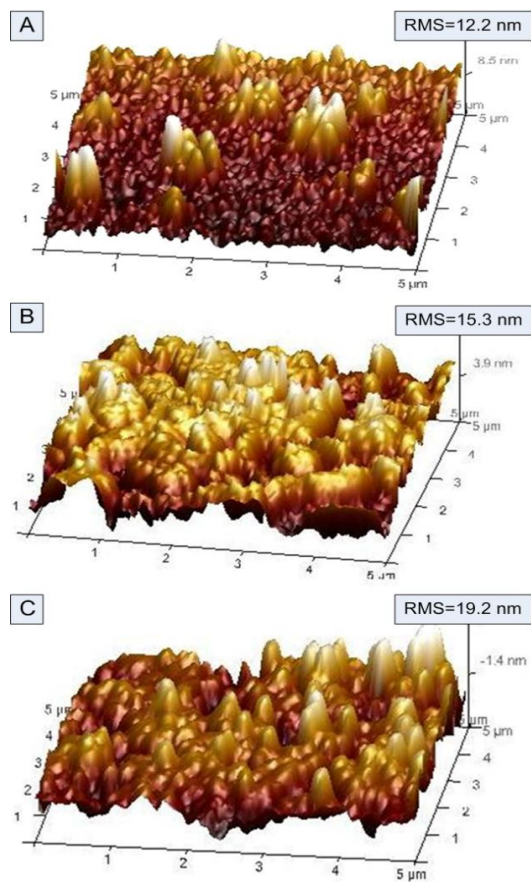


Figure 2. AFM (3-D) image of the as-grown and porous InGaN formed at different current densities. (A) as-grown, (B) 25mA/cm², (C) 50mA/cm².

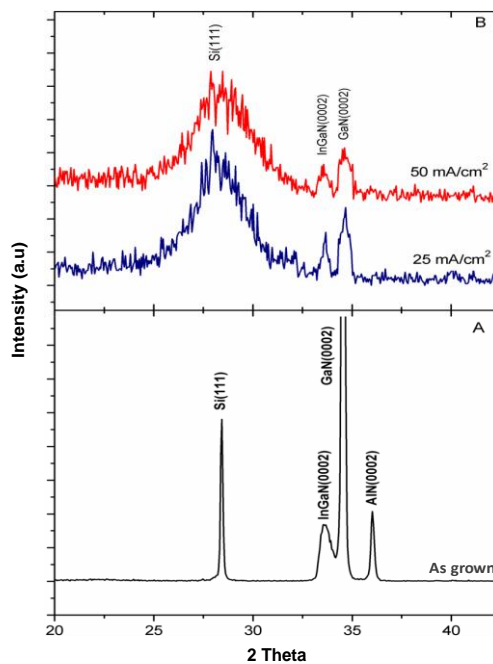


Figure 3. XRD of the as-grown and porous InGaN formed at different current densities. (A) as-grown, (B) porous samples.

The indium mole fraction (x) based on the chemical formula $\text{In}_x\text{Ga}_{1-x}\text{N}$ can be calculated using the XRD symmetric $\omega/2\theta$ scans of (0002) plane (Eq. 1) [16] and Vegard's law (Eq. 2) [17] as follows:

$$c = \frac{\lambda l}{2 \sin \theta} \quad (1)$$

where λ is the wavelength of the X-ray radiation (0.15406 nm), θ is the Bragg angle, and l is the Miller index;

$$x = \frac{c(\text{InGaN}) - c(\text{GaN})}{c(\text{InN}) - c(\text{GaN})} \quad (2)$$

where $c(\text{InGaN})$, $c(\text{GaN})$, and $c(\text{InN})$ are the actual c -plane lattice constants of InGaN, GaN, and InN, respectively. The value of the indium mole fraction of the InGaN epilayer was calculated to be equal to 0.27.

The mean crystallite size (D) of the film can be calculated using the Scherrer equation [18, 19] as follows:

$$D = \frac{0.9\lambda}{B \cos \theta} \quad (3)$$

where B is the FWHM (in radians), λ is the wavelength of the X-ray, and θ is the diffraction angle. Peak width (B) is inversely proportional to crystallite size (D) and the peak position. The FWHM and lattice constants of the as-grown and porous films are listed in Table 1.

Table 1. Peak position, lattice constants and other characteristics of the as-grown and etched samples.

Sample	Peak InGaN	Peak (2Theta)(°)	FWHM (2Thete)(°)	c (nm)	d (nm)	D (nm)	$\epsilon \times 10^{-3}$	$\Delta \epsilon$
As-grown		33.61	0.344	0.5329	0.2664	25.19	0.674	-
25 mA/cm ²		33.59	0.471	0.5332	0.2666	18.40	0.668	0.006
50 mA/cm ²		33.55	0.493	0.5338	0.2669	17.58	0.656	0.018

The strain (ϵ) along the c -axis can be calculated as follows:

$$\epsilon = \frac{c - c_0}{c_0} \times 100\% \quad (4)$$

where c and c_0 are the lattice parameters of the etched and as-grown $\text{In}_{0.27}\text{Ga}_{0.73}\text{N}$ thin films, respectively. The average crystallite size and the strain of the films were calculated using the equations

above, and the results are summarized in Table 1. The calculated compressive strain was found to decrease with the increase in current density of the porous film.

Fig. 4 shows the photoluminescence (PL) spectra of the as-grown and porous films, displaying the near band-edge emission of GaN at a wavelength of 365 nm. A PL wavelength emission peak at 556 nm is related to the as-grown sample. Slight blue shifts were observed in the porous films at wavelengths of 554.3 and 553.1 nm, which correspond to the etched films at 25 and 50 mA/cm², respectively.

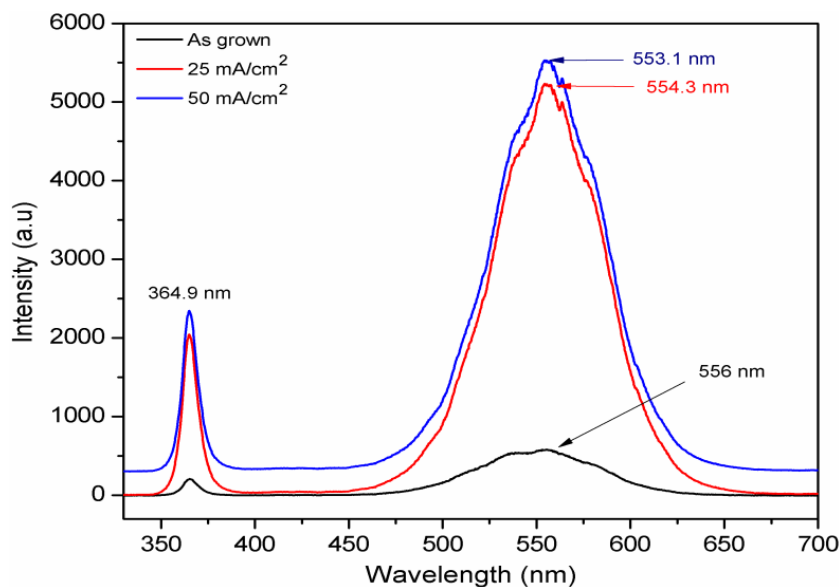


Figure 4. PL spectra of the as-grown and porous InGaN formed at different current densities.

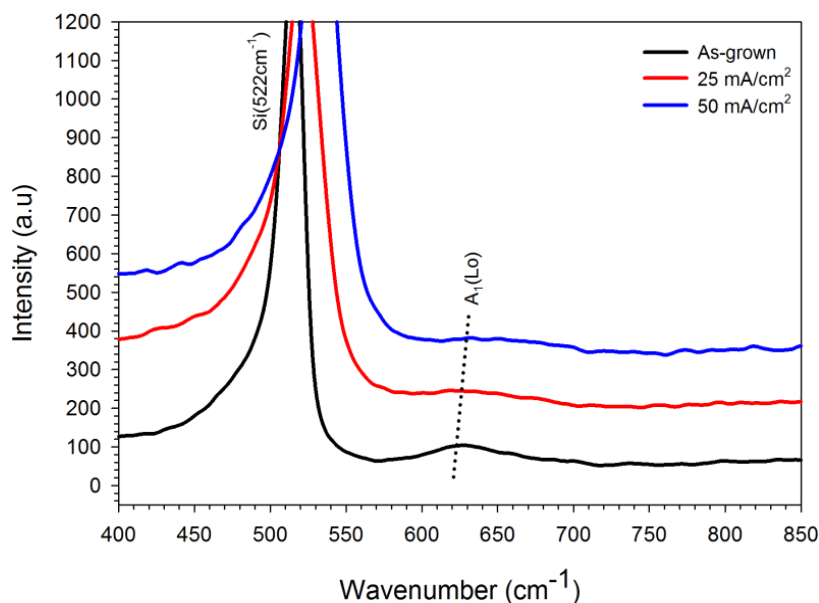


Figure 5. Raman spectra of the as-grown and porous InGaN with different current densities.

These shifts can be attributed to the change in current density. The PL peak intensity of the porous films was 10 times more than that of the as-grown film, indicating that porosity strongly affects peak intensity. The intensity of emitted light is known to be proportional to the number of emitted photons, and thus, the number of photons emitted by the porous film is much higher than the number emitted by the as-grown film.

High porosity-induced PL intensity can be explained by the extraction of strong PL via light scattering from the sidewalls of the sample crystallites [20]. Porous films have higher surface area per unit volume compared with as-grown films, and thus, the porous $\text{In}_{0.27}\text{Ga}_{0.73}\text{N}$ film provides much more exposure to the illumination of PL excitation lights for $\text{In}_{0.27}\text{Ga}_{0.73}\text{N}$ molecules. This phenomenon may result in a higher number of electrons taking part in the excitation and recombination process in porous films compared with the smaller surface area of the as-grown films [13]. The relatively wide statistical size distribution of the pores can be attributed to the broadening of the linewidth of porous films.

Fig. 5 shows the Raman spectra of the as-grown and porous $\text{In}_{0.27}\text{Ga}_{0.73}\text{N}$ films. One Raman phonon mode, namely, the $A_1(\text{LO})$ at 625.6 cm^{-1} of the as-grown film, was observed. Moreover, the porous films at 25 and 50 mA/cm^2 were observed to shift to higher frequencies at 627.3 and 630.6 cm^{-1} , respectively, relative to the as-grown film. This finding can be attributed to the compressive stress. One mode behavior for $A_1(\text{LO})$ is that the linewidth increases with increasing current density. No feature associated with the $E_2(\text{high})$ mode was observed above the luminescence background for all samples because $x < 0.60$. The broadening of the $E_2(\text{high})$ peak increased when the indium concentration (x) was decreased from 100% to 60% and damping at $x \approx 60\%$ [21]. Therefore, the $E_2(\text{high})$ mode did not appear in the Raman spectra of the samples because the sample contained indium concentration of only 27%. Moreover, a strong band at 522 cm^{-1} referring to the Si(111) substrate was also observed.

4. CONCLUSION

The $\text{In}_{0.27}\text{Ga}_{0.73}\text{N}/\text{Si}(111)$ thin film with thickness of 110 nm was prepared using the PA-MBE technique, with indium mole fraction of 0.27. The porous nanostructures of the $\text{In}_{0.27}\text{Ga}_{0.73}\text{N}$ layer were synthesized using the UV-assisted electrochemical etching method. These nanostructures can open a new and promising area in ternary III-nitride materials through the chosen suitable etching factors to enhance the structural and optical properties of thin films for optoelectronic devices. The pore size and roughness of the porous thin films increased with increasing current density, consequently decreasing the crystallite size and compressive stress. The change in current density had insignificant influence on the amount of peak shifting in the PL spectra, showing a clear increase in intensity. One mode behavior for $A_1(\text{LO})$ was observed from the Raman spectra, and the linewidth increased with increasing current density, suggesting the occurrence of stress relaxation.

ACKNOWLEDGEMENTS

Support from ERGS grant and Universiti Sains Malaysia is gratefully acknowledged.

References

1. D. Chen, B. Liu, H. Lu, Z. Xie, R. Zhang and Y. Zheng, *Electron Device Lett.*, 30 (2009) 605.
2. Z. Hassan, Y. Lee, F. Yam, K. Ibrahim, M. Kordesch, W. Halverson and P. Colter, *Solid State Commun.*, 133 (2005) 283.
3. F. K. Yam and Z. Hassan, *Materials Letters*, 63, 724 (2009).
4. A. Ramizy, Z. Hassan and K. Omar, *Sens. Actuators B*, 155 (2011) 699.
5. F. Yam, Z. Hassan and S. Ng, *Thin Solid Films*, 515 (2007) 3469.
6. A. Loni, L. Canham, M. Berger, R. Arens-Fischer, H. Munder, H. Luth, H. Arrand and T. Benson, *Thin Solid Films*, 276 (1996) 143.
7. E. Moyen, W. Wulfhekel, W. Lee, A. Leycuras, K. Nielsch, U. Gösele and M. Hanbücken, *Appl. Phys. A*, 84 (2006) 369.
8. X. Guo, T. Williamson and P. Bohn, *Solid State Commun.*, 140 (2006) 159.
9. G. Korotcenkov and B. Cho, *Crit. Rev. Solid State Mater. Sci.*, 35 (2010) 1.
10. F. Yam, Z. Hassan and A. Hudeish, *Thin Solid Films*, 515 (2007) 7337.
11. F. Yam, The Study Of Gan Materials For Device Applications, in: Universiti Sains Malaysia, Malaysia (2007).
12. K. Beh, F. Yam, C. Chin, S. Tneh and Z. Hassan, *J. Alloys Compd.*, 506 (2010) 343.
13. K. Al-Heuseen, M. Hashim and N. Ali, *Appl. Surf. Sci.*, 257 (2011) 6197.
14. K. Al-heuseen, M. Hashim and N. Ali, *Physica B*, 405 (2010) 3176.
15. O. Volciuc, E. Monaico, M. Enachi, V. Ursaki, D. Pavlidis, V. Popa and I. Tiginyanu, *Appl. Surf. Sci.*, 257 (2010) 827.
16. A. Hussein, S. Thahab, Z. Hassan, C. Chin, H. Abu Hassan and S. Ng, *J. Alloys Compd.*, 487 (2009) 24.
17. C. Van de Walle, M. McCluskey, C. Master, L. Romano and N. Johnson, *Mater. Sci. Eng., B*, 59 (1999) 274.
18. A. Burton, K. Ong, T. Rea and I. Y. Chan, *Microporous Mesoporous Mater.*, 117 (2009) 75.
19. B. Cullity, Elements of X-ray Diffraction, 2nd ed., Addison-Wesley publishing Co. Inc., Boston 1978.
20. A. Vajpeyi, S. Tripathy, S. Chua and E. Fitzgerald, *Physica E*, 28 (2005) 141.
21. V. Davydov, A. Klochikhin, V. Emtsev, A. Smirnov, I. Goncharuk, A. Sakharov, D. Kurdyukov, M. Baidakova, V. Vekshin and S. Ivanov, *phys. status solidi B*, 240 (2003) 425.